Integration of laser profiler feedback into FIM for additive manufacturing in construction

Simon Leon Espinosa[1], **Martin Slepicka**[1] **and André Borrman**[1]

[1]Chair of Computational Modeling and Simulation, Technical University of Munich, Germany

simon.espinosa@tum.de, martin.slepicka@tum.de

Abstract -

This research delves into the utilization of laser profiling technology within the realm of Three-Dimensional (3D) printing in the construction industry. The primary emphasis is on achieving a seamless integration of Fabrication Information Modeling (FIM), Additive Manufacturing (AM), and Digital Twinning (DT). The study involves the capture of precise measurements at various stages and storing them as Point Cloud (PC) data. Moreover, the objective is to transform operational planning and enhance real-time "as-built" data generation by intricately mapping shape and height deviations and storing the corresponding data in the FIM model.

Keywords -

BIM; FIM; RTDE; Cyber-Physical-Systems; Digital Twin

1 Introduction

In comparison to other industry sectors, the construction industry has traditionally faced challenges in improving productivity. However, recent advancements in key technologies are poised to address this longstanding issue. Building Information Modeling (BIM), Additive Manufacturing (AM), and Digital Twining have already made their mark, offering transformative possibilities. In this context, Fabrication Information Modeling (FIM) [1] was introduced as a bridge between digital design and automated manufacturing in order to further expand the level of automation in the construction industry and thus contribute to the fourth industrial revolution, commonly referred to as "Industry 4.0". [2]

Each of these technologies plays a unique role in reshaping the construction landscape. BIM is a digital design methodology for creating and using digital building models that are intended to represent the physical and functional properties of a building as accurately as possible [3]. AM helps to automate manufacturing on-site and off-site and enables the production of components with complex geometry and improved material efficiency. As an intermediary layer between BIM and AM, FIM manages fabrication information, facilitating a seamless transition of 3D information into discrete two-dimensional (2D) data for layer-by-layer manufacturing [1]. Digital Twining (DT) ensures real-time synchronization between physical objects and digital models [4].

Industry 4.0 is characterized by increasing digitization, smart manufacturing, and customization, driving the development of the construction industry from planning to construction, focusing on quality control through sensors and thorough planning. As technology integration increases, DT and AM methods are employed to update digital models and automate construction processes. Both technologies reduce the need for manual labor by automating repetitive or controllable tasks and thus enhance productivity [2]. However, along with all the advantages of AM methods, there are also limitations. One of the problems with AM is the lower reliability compared to traditional manufacturing methods, especially in terms of deviations between the as-printed and as-designed state, if the AM process is not adequately controlled by feedback [5]. In this context, this study focuses on enabling digital twining methods for AM, aiming to provide real-time monitoring for improved decision-making.

The data structure of FIM models was designed based on the BIM exchange data format Industry Foundation Classes (IFC) and can contain various model representations side by side. This means that a FIM model can include both the as-designed data extracted from the BIM model, fabrication information, and later sensor data (as-printed data). Based on such a data foundation, with a system for real-time data exchange [6], and with the sensor integration proposed in this study, it is feasible that FIM can be used for cyber-physical systems (CPS) [7].

In the following, the technologies on which this work is based and their current status are first described in section 2. Subsequently, the proposed methodology is detailed in section 3. Finally, information on this methodology's impact on the industry is provided in section 5.

2 Background

The study presented in this article examines how sensor feedback can be integrated into FIM-based additive manufacturing. To this end, an insight into the FIM methodology and the underlying data structure is first provided. After this, the optical sensor system used in this work is described.

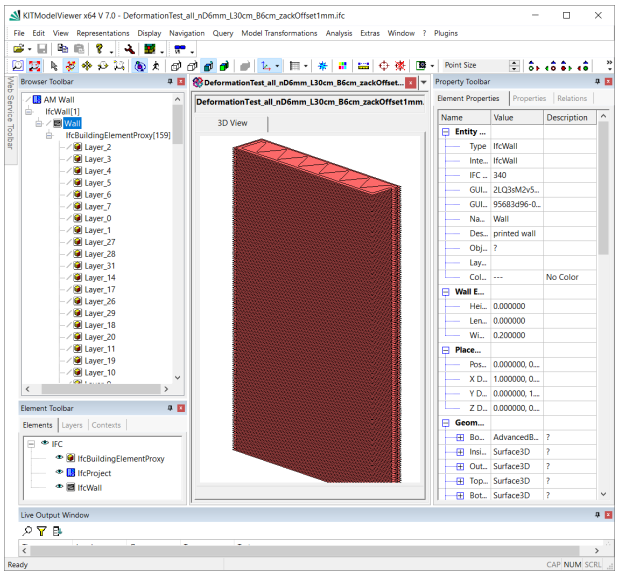

Figure 1. Visualization of the FIM-IFC data.

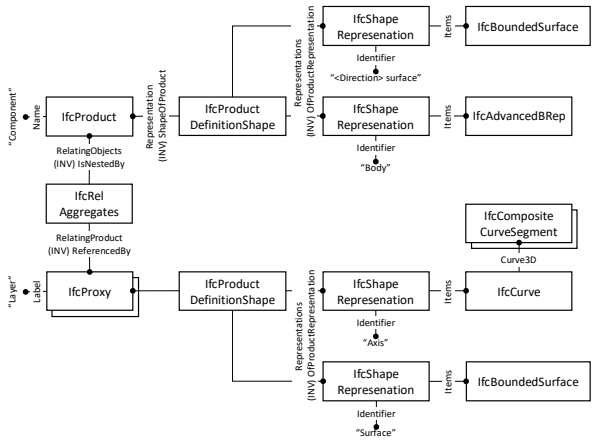

Figure 2. Express-G diagram of the FIM data structure, after [1].

2.1 Fabrication Information Modeling (FIM)

According to Slepicka et al. [1], FIM is an intermediate layer between digital design and automated manufacturing. The FIM framework implemented by Slepicka et al. [1] can be used to derive manufacturing information from digital models, such as a BIM model, which can be used directly in manufacturing. For this purpose, the tool path for creating the object is generated from the extracted information of the digital model and enriched with manufacturing data.

With the FIM Framework, components can be extracted from a BIM model and automatically enriched with manufacturing information using a pattern-based algorithm. The 3D geometry data, if not already given as boundary representation (B-Rep), is converted into a B-Rep model, and the corresponding boundary surfaces are topologically mapped. A pattern-based path planning algorithm is then executed to generate a C2-continuous tool path using the boundary surfaces and slicing planes. Additionally, to avoid rapid tool acceleration, e.g., in tight curves, a velocity profile is generated depending on the curvature of the path. [1]

The data generated with FIM, i.e., B-Rep, slicing planes, path, and speed profile, are formatted in the BIM exchange data format, the Industry Foundation Classes (IFC). The different data is attached to the same component as different representations (`IfcShapeRepresentation`). The component to be printed (e.g., `IfcWall`) is represented as an assembly (`IfcRelAggregates`) of layers (`IfcBuildingElementProxy`), each of which is described by its slicing surface (`IfcSurface`) and the corresponding tool path (`IfcCompositeCurve`) (see figs. 1 and 2) [1].

The data structure just described, in particular the ability to access the individual surfaces of the component, has several functions. As described above, the boundary and layer surfaces are used for path planning. However, the corresponding surfaces can also be used as an aid for simulation purposes [8]. Moreover, the subject of this study is the possibility of using these surfaces as a reference for "as-printed" measurements.

2.2 Geometric data acquisition

There are various optical sensor systems for 3D geometry acquisition, e.g., active and passive stereo cameras, terrestrial LiDAR, structured light sensors, and laser profilers. This study focuses on laser profiling, a technology in which a laser line is projected onto an object to be measured, which is captured using a camera via triangulation. As in the study by Chen et al. [9], in which this technology was used for quality assurance in an AM process, a laser profiler is also attached to the robotic arm carrying out the AM process in this study in order to be able to capture the component geometry during the printing process.

The sensor works by projecting a laser line on the object to be measured and capturing the reflection to create a 2D profile, as illustrated in fig. 3. The object is scanned, and a 2D version and its surroundings are obtained. It is important to note that only the reflected data can be captured; therefore, some parts of the measured object may be occluded and not visible to the scanner. For this reason, the scanning path and orientation are crucial for the results.

This type of sensor is commonly used in production lines, where the sensor is mounted stationary, and the objects to be measured are moved under the sensor on a conveyor belt. In this way, individual line measurements

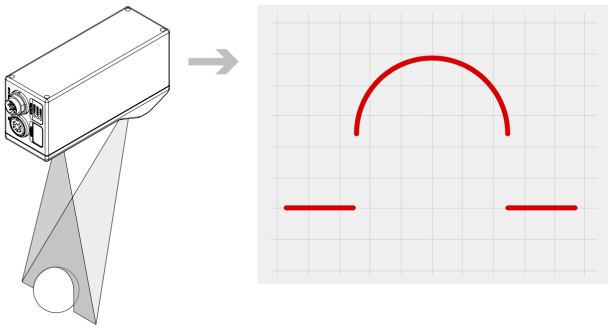

Figure 3. Functional principle of the laser profiler (left) and the corresponding measurement result (right) [10].

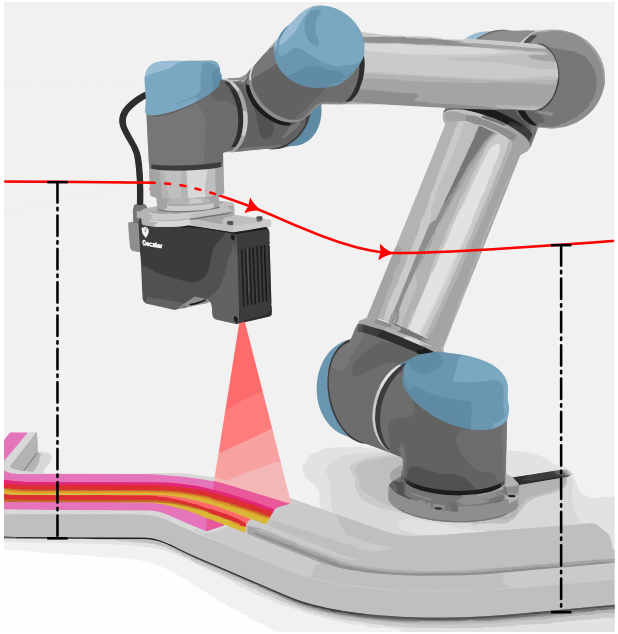

Figure 4. Robot mounted laser profiler on a path at a constant distance to the base surface.

can be combined to provide a surface measurement. However, as Chen et al. [9] show, a laser profiler can also be mounted on a robot to carry out surface measurements. A necessary prerequisite for accurate measurement is that the robot guiding the sensor moves as uniformly as possible over the object to be measured, as stated by our laser profiler documentation [10], see fig. 4.

If the distance between the sensor and the ground is known, the sensor output can be calibrated so that the height of the measured object can be returned in relation to the ground. This allows a matrix with height values to be created from several line profiles, i.e., a 2.5D representation of the object. Within the laser line, there is a resolution depending on the distance to the object, and from one laser line to another laser line, there is a resolution depending on the speed of movement of the sensor (if robot-mounted).

3 Method

As previously indicated, the hypothesis in this study is that laser profiling can be integrated into the FIM methodology (cf. section 2.1) for "as-printed" data feedback. The idea is that the manufacturing information available in a FIM model can be used to generate robot trajectories for a scanning process with a laser profiler (cf. section 3.1). The data captured along these trajectories needs to be post processed by removing unwanted data (cf. section 3.2) and transforming it into manageable packages (cf. section 3.3), which can be fed back into the FIM model (cf. section 3.4). In both cases, the boundary and layer surfaces stored in the FIM model are used for this purpose (cf. figs. 1 and 2).

3.1 Scan planning

As already indicated in section 2.2, the sensor must be moved at a constant speed along a robot trajectory at a constant distance from a reference plane so that a scanning process with a laser profiler can deliver usable results (cf. fig. 4). To create such a robot trajectory, the corresponding surface geometry of the part to be measured can be taken from the FIM model. If, for example, a printed layer is to be checked, the corresponding layer surface can be used. When measuring the overall geometry, on the other hand, the individual surfaces of the B-Rep representation can be used. Using the profile width of the sensor, the desired surface can be divided into suitable segments from which the central isocurve can be derived and shifted to a constant distance from the surface using an offset. It is important to note that the offset curves created in this way must be extended beyond the corresponding area at both ends. A robot needs some time to accelerate to a constant speed, and the quality of the measurement with the laser profiler is impaired during acceleration. The extended curves create a buffer zone to compensate for this. Additionally, this extended area for measurement enables the detection of material outside the designed range (over-extrusion).

3.2 Data filtering

As previously described in section 3.1, the paths for the scanning process must be longer than the actual object geometry. Furthermore, if a surface had to be recorded in several segments, several data sets must be combined into one. This means that a few measured lines have to be removed, and lines have to be trimmed.

In addition, invalid measured values must also be removed. A measured value is considered invalid if it lies within the range of another measurement (e.g., in the previous layer) or far outside the expected range (background). The decision as to whether a measured value is considered invalid is determined in this study via a threshold value. By defining a region of interest (ROI) that incorporates the designed geometry, including a margin of error, unwanted data points can be removed from the captured data. Using the FIM data, it is possible to define this ROI in the form of a volume in space; every measured value outside this volume can be excluded. Additionally, this method simplifies assigning the measured values to the correct "as-designed" surface.

3.3 Deviation maps

The sensor data must be correlated with the geometric information in the FIM model to enable data feedback later. If the sensor is operated as described in section 3.1, deviations or heights are measured by the sensor in relation to the reference plane used, i.e., to the "as-designed" surface that was used to generate the robot trajectory. As described in section 2.2, the sensor output is then a matrix with the height values at the equally distributed measurement positions. In this respect, the measured data can also be interpreted in relation to surface coordinates (UV coordinates). Effectively, only the individual matrix positions of the measured values need to be mapped to the UV coordinates of the reference surface, i.e., instead of assuming a fixed Cartesian distance between matrix cells, a parameter distance can also be considered (cf. section 3.4).

If the measured height value is then coded in a color value, a heat map (or deviation map) can be derived (cf. figs. 9 and 10). The heat map is designed to show the deviation in two different scales for a more intuitive visualization. A cold scale visualizes the over-extruded sections (height values larger than zero), while the under-extruded sections (height values smaller than zero) are visualized by a warm scale.

Similar to the height deviation map, which visualizes the deviation of the measured values in the normal direction to the reference surface, a second deviation map can also be created for each of the layer surfaces, which shows the deviations from the "as-designed" printing path. These are then deviations tangential to the reference surface. These deviations are determined by filtering the height values of the sensor matrix using binary filtering and the "as-designed" position, which is determined using the printing path in the FIM model. If the "as-designed" and "as-printed" data are superimposed, different areas can be color-coded depending on whether too many, too few, or exactly the right data points were detected in the "as-printed" data set. This approach enables a detailed analysis, distinguishing between instances where the material is present in unintended locations and situations where the material is absent from anticipated positions.

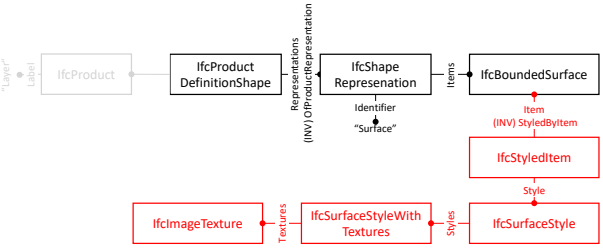

Figure 5. Data structure for attaching a texture to a geometry.

3.4 Data feedback

Both deviation maps described in the previous section are already created in such a way that the data is referenced to the surface geometries stored in the FIM model. Accordingly, the maps can be attached to the data model as a texture without further revision, as already indicated above. The heat map textures can be attached to the corresponding surface as `IfcStyledItem` in the FIM model. The necessary additions to the data model are illustrated in fig. 5 (additions in red).

4 Experimental validation

In order to validate the methodology described in section 3, various tests were carried out on a small-scale setup. In the following, the setup is first described (cf. section 4.1), and then the necessary implementations are explained (cf. section 4.2). Finally, the results obtained are presented section 4.3.

The experimental part of this research was conducted in the scope of the master's thesis by Espinosa [11].

4.1 Setup

To validate the methodology proposed in this study, a clay 3D printing manufacturing setup was used. In extrusion-based 3D printing, clay behaves similarly to concrete and is well suited for conducting preliminary laboratory tests. Figure 6 shows this setup. It consists of two Universal Robots arm robots, a UR10e and a UR5e, the former equipped with a Stoneflower3D clay extruder and the latter with a Gocator 2330 laser profiler (Resolution Z: 0.006 mm, Clearance Distance: 90 mm, Measurement Range: 80 mm, Field of View: 47–85 mm). Both robots are securely positioned on a "level" table (cf. section 4.3). Additionally, the UR5e (in the backside of fig. 6) is placed on a longitudinal axis for extended reach.

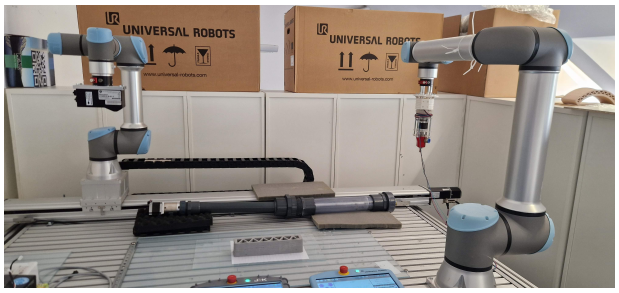

Figure 6. Full setup at home position. UR10e robotic arm outfitted with a stoneflower3D clay extruder on the right. And on the left a UR5e on a SlideKit linear axis outfitted with a Gocator 2330 laser profiler.

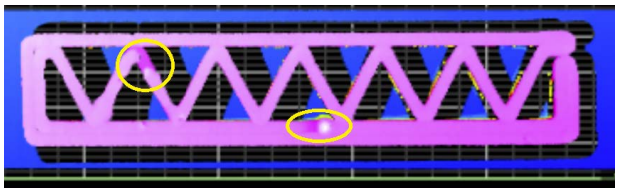

Figure 7. Imported raw sensor data of a layer scan (Layer 14). Even before post-processing, ROIs can be identified (marked by the yellow circles). Visible are a defect (left) and the transition from the previous printing layer (right).

Each robot undergoes calibration, and a transformation matrix is computed to establish a correlation between their individual positions. This matrix enables a cross-reference of their respective coordinate systems, which is crucial for aligning the "as-built" structure with the "as-designed" model. Beyond alignment, this transformation matrix plays a pivotal role in precisely situating the "as-built" model on the table, ensuring accurate positioning.

The alignment of these two data sets is facilitated by the utilization of a Real-Time Data Exchange (RTDE) module by Slepicka et al. [6] in both UR robots, enabling precise positioning for their respective tasks. This synchronization ensures that the position of each robot is consistently known, not only facilitating alignment but also serving as a valuable resource for the calibration of measurements throughout the entire process.

The Gocator sensor is securely attached to the robot, and the scanning process is executed by moving the sensor from the start to the finish point using the URCap provided by the sensor's manufacturer, LMI [10, pp. 1038–1063]. The connection between the Gocator and the UR robot is established through the Dynamic Host Configuration Protocol (DHCP).

Continuous robot movement ensures that the Gocator sensor moves at a speed of 60 mm/s during scans. To ensure consistent scanning performance, the robot must reach maximum speed before reaching the scanning area. This particular requirement enables accurate and reliable data capture throughout the scanning process.

4.2 Implementation

The computational tools for the Lab setup are implemented using Python and consist of two main classes to control the information flow. One class effectively manages the data import from the Gocator sensor ("as-printed" data) and all the coordinate information of it. The other class manages the data flow from and to the FIM model, including the designed path information, layer information, desired height, and scale. In addition, multiple utilities were implemented to process and communicate sensor and FIM data.

The current implementation has no tools to automate the scanning process and the data flow. During the 3D printing process, the scanning has to be triggered via a manual command while the printing process has to be paused. The Sensor then stores the measured raw data in a CSV file, which can then be utilized with the Python tool introduced in the previous paragraph.

The raw sensor data should first be organized to utilize the scan data properly. For this, it is necessary to first reformat the data into arrays and filter out undesired data points. Via a `fromCSVtoCloud` function the data in the CSV file is read and converted to a list of point coordinates, essentially a point cloud (cf. fig. 7). In this format, the data can easily be filtered as described in section 3.2 by performing inside-outside tests for each point with the specified ROI.

The filtered sensor data can then be processed by the Python tool into the deviation maps by comparing the sensor data with the FIM data. All the required processing for creating deviation maps was performed by utilizing image processing tools of the *OpenCV* module for Python. Application examples of the implementation described above can be seen in the next section.

4.3 Results

To demonstrate the proposed method, a straight wall segment was printed in model scale, as illustrated in fig. 8, and scanned with a Gocator laser profiler at certain stages of the process. The resulting data was then processed with the tools described in the previous section. During the manufacturing process of the model wall, the process was paused after finishing 7 layers at a time to perform a layer scan. After completing the manufacturing process, another scan was performed to capture the front surface of the wall.

The object shown in fig. 8 was printed until the clay

cartridge was empty with the purpose of generating large deviations from the "as-designed" data. The final layer of this print provided an exciting testing ground for the geometry-capturing method. The following will show processed layer scans of the 14th and 21st layers (height and shape deviation) and a lateral scan of the completed wall (only height deviation).

Height deviation maps

First, the height deviation map of the 14th layer of the example wall is shown, then that of the 21st layer, and finally, the deviation map of the lateral scan:

In fig. 9, many details about the printing process are already visible. The blue color on the upper left indicates over-extrusion, and the red on the lower right indicates under-extrusion. However, there seems to be an axis on which the correct layer height has been printed. This observation can be explained by the fact that the UR10e (printing robot) is slightly tilted in relation to the table. This slight tilt ($< 0.5°$) results from imperfections in the lab table and could be accounted for by calibrating the tool position of one robot with respect to the base coordinate frame of the other. This positioning issue was revealed by the experiments but left uncalibrated to illustrate the system's sensitivity.

Other areas of interest are the two sections colored in deep red. One of these sections (lower part of the image) represents the area in which the printer transitions to the next layer, while the other section (upper left) shows a filament tear caused by an air bubble in the material feed. However, the threshold filter was not set accurately in the filament tear section, as this section should be blank (no information on the lower layers should be available).

In fig. 10, it is clearly visible that the layer has not been printed entirely, as large parts of the expected shape are missing. These values have been removed by the threshold filter, as they belong to the layer below. However, similar to layer 14 (cf. fig. 9), due to the tilt, not all the values that should belong to the previous layer were removed (dark red colored part in the upper left of fig. 10).

Figure 11 shows a representative part of the deviation map derived from the lateral scan. It was trimmed for visualization purposes. As in the previous figures, defects are clearly visible; Deep red spots indicate filament tears.

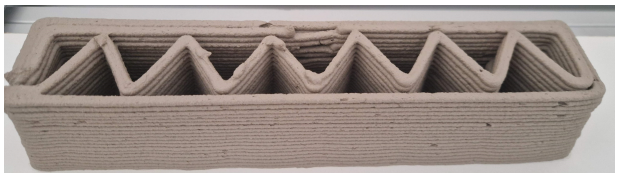

Figure 8. Completed clay wall.

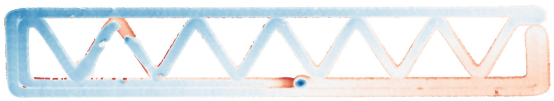

Figure 9. Height deviation map of the 14th layer during the printing process.

Figure 10. Height deviation map of the 21st layer (the last layer) shortly after the printing process.

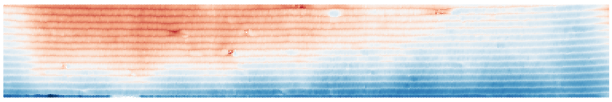

Figure 11. Trimmed deviation map of the lateral scan after completion of the printing process.

In addition, it is visible that the lower layers seem to be over-extruded. However, this excess material could be explained by the material behavior: The more material is deposited on top, the more weight is carried by the lower layers, which compresses the lower layers and pushes the material outwards.

Shape deviation maps

Same as before, for the height deviation maps, the shape deviation is illustrated for the 14th and 21st layers.

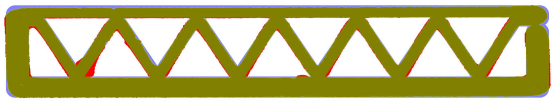

Figure 12. Shape deviation map of the 14th layer during the printing process.

Figure 13 illustrates the shape deviation of the 14th layer, derived from a scan captured during a pause in the manufacturing process. In green, the "as-printed" geometry matches with the "as-designed" model (neglecting any height deviations); in red, too much material and in blue, insufficient material was deposited. As this deviation map was derived from the height deviation map (cf. fig. 9), the issue with the unfiltered data, as mentioned before, persists, and thus the filament tear is not recognized in this deviation map.

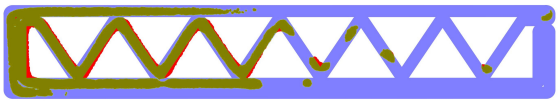

Figure 13. Shape deviation map of the 21st layer during the printing process.

Figure 13 depicts the shape deviation of the 21st layer. Similar to before, it is clearly visible that more than half of the layer is missing. But as with the shape deviation map of layer 14 (previous figure), there is the same issue with the wrongly unfiltered data that belongs to the layer below.

4.4 Discussion

A significant difficulty in data post-processing is the adjustment of the filter. Employing an overly aggressive filter risks losing crucial information, while a too-lenient filter introduces noise or retains undesired data, as observed in fig. 9. In either scenario, the accuracy of the results is compromised, incorporating inaccurate data. Given the sensor's high resolution, substantial noise is not anticipated; instead, the focus is on filtering out scanned information from undesirable positions, e.g., when performing layer scans and data from the previous layer is retained. In layer scans, the deviation map of the previous layer can be utilized to filter the captured point cloud of the current layer in order to remove points that correspond to the previous layer. In the example shown, this was not possible because not every layer was scanned.

As indicated in the previous section, the results showed that the positioning of the two robots with respect to each other did not perfectly match. However, this was not a problem in developing the proposed method; instead, it underlined its usefulness. In future experiments, when the accuracy of the "as-printed" geometry data is important, care must be taken to ensure the system is correctly calibrated.

Additionally, it's important to note that some applications of this study may not be seamlessly extrapolated to a larger scale. A notable example is the handling of layer information, where, in the current study, all layer data is encapsulated within a single scan. In the context of a larger model, the process necessitates multiple scans, subsequently requiring an alignment of various scans.

5 Conclusion

One of the selling points of AM in construction is that it can manufacture components resource-efficiently. However, as mentioned in section 1, AM methods can be unreliable and fail due to incorrect parameter settings, operating errors, or environmental influences. To ensure error-free, high-quality, and resource-efficient 3D printing, it is almost imperative that the "as-printed" and "as-designed" states are continuously compared with each other.

As illustrated in section 4.3, even with a poorly calibrated system, a lot of helpful information can be extracted from the "as-printed" data to react early to impending problems. Although the system shown is currently not fully automated, it is still possible to recognize the possibilities this system can offer if all components are fully automated. With "as-designed" and "as-printed" data closely intertwined in the FIM data structure, data accessibility for automated quality control will not be an issue. The component's geometry, semantics, fabrication information, and captured "as-printed" data can be stored side-by-side with FIM.

Since the results are stored in textures, it is possible to store several recorded states of the corresponding component and visualize them independently so that different information can be stored and displayed in the same place. Visually embedding post-processed scan results within the FIM model provides a comprehensive and intuitive representation of the manufactured component, enhancing the interpretability of any measurements performed on it and enabling the storage of the manufacturing history of the object. Overall, this method will make it possible to develop the FIM methodology into a cyber-physical system.

Acknowledgments

The authors gratefully acknowledge the financial support of the Deutsche Forschungsgemeinschaft (DFG) in the frame of the Transregio 277 "Additive Manufacturing in Construction" (Project 414265976) and the Priority Program 2187 "Adaptive modularized constructions made in a flux" (Project 423969184).

References

[1] Martin Slepicka, Simon Vilgertshofer, and André Borrmann. Fabrication Information Modeling: interfacing building information modeling with digital fabrication. *Construction Robotics*, 6(2):87–99, 2022. ISSN 2509-8780. doi:10.1007/s41693-022-00075-2. URL `https://doi.org/10.1007/s41693-022-00075-2`.

[2] Orsolya Nagy, Ilona Papp, and Roland Zsolt Szabó. Construction 4.0 organisational level challenges and solutions. *Sustainability*, 13(21):12321, 2021.

[3] André Borrmann, Markus König, Christian Koch, and Jakob Beetz. Building information modeling:

Why? what? how? In *Building information modeling – Technology Foundations and Industry Practice*, pages 1–24. Springer, 2018.

[4] Rafael Sacks, Ioannis Brilakis, Ergo Pikas, Haiyan Sally Xie, and Mark Girolami. Construction with digital twin information systems. *Data-Centric Engineering*, 1:e14, 2020.

[5] Yanzhou Fu, Austin Downey, Lang Yuan, Avery Pratt, and Yunusa Balogun. In situ monitoring for fused filament fabrication process: A review. *Additive Manufacturing*, 38:101749, 2021.

[6] M. Slepicka, J. Helou, and A. Borrmann. Real-time data exchange (rtde) robot control integration for fabrication information modeling. In *Proceedings of the 40th ISARC*, Jul 2023. doi:https://doi.org/10.22260/ISARC2023/0016.

[7] Yang Liu, Yu Peng, Bailing Wang, Sirui Yao, and Zihe Liu. Review on cyber-physical systems. *IEEE/CAA Journal of Automatica Sinica*, 4(1):27–40, 2017.

[8] O. Oztoprak, M. Slepicka, A.L. Aninger, S. Kollmannsberger, E. Rank, and A. Borrmann. Linking fabrication information modeling and finite cell method for simulating the behavior of additively manufactured building components. In *EG-ICE Conference*, London, United Kingdom, 2023.

[9] Lequn Chen, Xiling Yao, Peng Xu, Seung Moon, and Guijun Bi. Rapid surface defect identification for additive manufacturing with in-situ point cloud processing and machine learning. *Virtual and Physical Prototyping*, 16, 10 2020. doi:10.1080/17452759.2020.1832695.

[10] LMI. Gocator line profile sensors – user manual. On-line: `https://d3ejaiy6gq5z4s.cloudfront.net/manuals/gocator/gocator-4.1/pdf/15159-4.1.4.12_MANUAL_User_Gocator-2300-2880-Series.pdf`, Accessed: 25/12/2023.

[11] S. Espinosa. Integration of laser profiler feedback into fim-based additive manufacturing in construction. Master's thesis, Technische Universität München, Sep 2023.